CO-SIMULATION OF AN AXIAL FLOW COOLING FAN AND A SUPERCRITICAL CO_2 AIR-COOLED HEAT EXCHANGER

Francois D. Boshoff, Sybrand J. van der Spuy,
Johannes P. Pretorius, Ryno Laubscher

Stellenbosch University, South Africa

SUMMARY

An axial flow fan has been designed for the air-cooled heat exchanger (ACHE) of a concentrated solar power plant, based on a supercritical carbon dioxide (sCO_2) Brayton cycle. This paper presents a high-fidelity co-simulation method, which simultaneously solves the air- and sCO_2-side flows through the ACHE and fan. The air-side flow is modelled using three-dimensional computational fluid dynamics, while the sCO_2 flow is solved using a one-dimensional thermofluid network model. The co-simulation is used to determine the thermal performance of the ACHE and to investigate the effects of non-uniform air flows on the behaviour of the sCO_2 in the tube bundle.

INTRODUCTION

Supercritical carbon dioxide (sCO_2) Brayton cycles for power generation is a new technology, that promises many improvements over steam Rankine cycles. These include increased plant thermal efficiencies [1], compact turbomachinery [2], and the fact that fluids at ambient conditions, such as air and water, function well as coolants for sCO_2 [3]. These benefits have caused research into the sCO_2 Brayton cycle to increase over the last two decades, including its application to a range of energy sources such as nuclear, geothermal and concentrated solar power (CSP).

The use of sCO_2 as working fluid complicates the design and control of such plants. Firstly, CO_2 must remain above its critical temperature and pressure, at 30.98°C and 7.38 MPa respectively, to remain supercritical. If the temperature or pressure drops below these values, the fluid could experience drastic changes in its fluid properties, leading to a decreased cycle efficiency, unpredictable behaviour or even damage to downstream components [2]. The fluid properties of sCO_2 are also very sensitive to temperature and pressure variations, particularly near the critical point, and are therefore difficult to predict accurately.

Various models of sCO_2 Brayton cycles have been reported in the literature which discretises the sCO_2 flow path to account for local variations in fluid properties [2, 4, 5, 6]. While these provide a

good understanding of the overall power cycle performance, it gives very little practical information on the performance of individual components, such as turbomachinery and heat exchangers. There are also very few experimental models of sCO_2 power cycles reported in the literature.

The work of Deshmukh et al. [2] investigates a 100 MW CSP plant based on the sCO_2 Brayton cycle, which uses an air-cooled heat exchanger (ACHE) for cooling. In particular, this work considers the transient effects of air temperature changes on the sCO_2 in the finned-tube bundle, which begins to provides more detail on how such a system would behave. To build on this understanding of ACHE units for sCO_2-based CSP plants, and to provide a practical example, Boshoff et al. [7, 8, 9] develops a detailed ACHE design for a similar CSP plant.

In their work, Boshoff et al. designs a bespoke axial flow cooling fan, specifically for use in this ACHE [7]. The resulting design features an unusual configuration for an axial flow fan, with a large hub-to-tip ratio of 0.51, and blades with very little twist. The performance of the fan is evaluated using both Computational Fluid Dynamics (CFD) and experimental tests of a 1:4.78 scale model of the fan [8]. The aerodynamic interaction between the fan and the finned-tube bundle is also investigated using CFD, assuming isothermal flow [9]. This model assumes that the heat transferred from the sCO_2 to air has no effect on the air-side flow, and can therefore be neglected. Based on the results, Boshoff et al. finds that the overall cooling air flow rate is only 3.6% below the required operating point, but the distribution of this cooling air throughout the bundle is highly non-uniform.

Considering the sensitivity of sCO_2 to temperature changes near the critical point, it is unclear what the effect of this non-uniform cooling air distribution will be on the overall thermal performance of the ACHE, and on the sCO_2 within the tubes. It is also possible that the non-uniform cooling could cause the sCO_2 in some tubes to be cooled excessively, to below the critical point, leading to drastic changes in fluid properties. Therefore, in the current work, a co-simulation model is developed which simultaneously solves the air-side flow field using three-dimensional CFD, implemented in ANSYS Fluent, and the sCO_2-side flow field using a one-dimensional thermofluid network method, implemented in a Python script. Communication between these models is managed by the *PyFluent* module. This co-simulation approach allows for the estimation of the overall thermal performance of the ACHE, and demonstrates the effect of the fan's non-uniform cooling air distribution on the sCO_2 flow in the finned-tube bundle.

AIR-SIDE MODEL

The ACHE's finned-tube bundle consists of 1160 finned tubes positioned above six fans. Each tube is bent to obtain eight vertical passes, with each pass spanning across the same two fans, as shown in Figure 1. The computational domain is defined by dividing the entire ACHE into thirds, each of which contains two fan units and roughly 386.7 tubes, with the assumption being that flow in each of these segments of the ACHE is identical. Both the air- and sCO_2-side flow fields are discretised, but uses different discretisation resolutions and methods.

The air-side flow through the two fan units is modelled using a three-dimensional CFD method, implemented in ANSYS Fluent. Each fan unit is split into five sub-domains: an inlet, fan rotor, plenum chamber, tube bundle and outlet. A hexahedral mesh is generated for the fan rotor sub-domain using ANSYS Turbogrid. Tetrahedral meshes are generated for the inlet, plenum and outlet sub-domains, using ANSYS Meshing, which are converted to polyhedral meshes after importing into ANSYS Fluent. Finally, a hexahedral mesh is generated for the tube bundle sub-domain. The assembled mesh is shown in Figure 1.

To simplify the air-side flow field solution, the complex geometry of the finned-tube bundle is neglected. Instead, the tube bundle effects are modelled using three distinct methods: Firstly, the flow

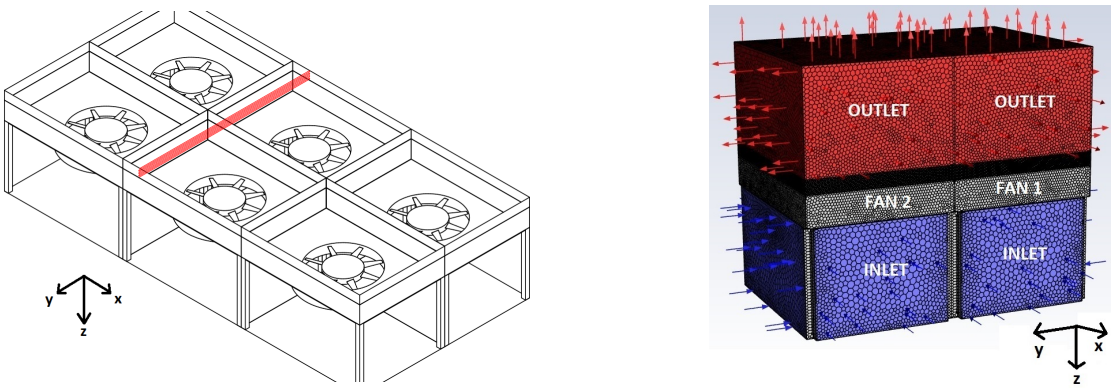

Figure 1: Position of a tube above two fans in the ACHE (left) and the assembled air-side CFD mesh containing two fan units (right)

straightening effect of the tube bundle is modelled using a Porous Media Model, with the x- and y-direction inertial resistance factors given a value of 1000. This high inertial resistance results in air flowing directly upwards (negative z-diretion) through the bundle.

Secondly, the static pressure drop of the air flowing through the tube bundle is modelled using z-direction momentum source terms. The value of these source terms are calculated using a User Defined Function (UDF). For each cell, the static pressure drop is calculated using the empirical correlation by Ganguli [10], expressed as:

$$\Delta p = \frac{2N_r G_{crit}}{\rho}\left[1+\frac{2e^{-\frac{P_t-d_f}{4d_o}}}{1+\frac{P_t-d_f}{d_o}}\right]\left[0.021+13.6\frac{d_f-d_o}{Re(P_f-t_f)}+0.252\left(\frac{d_f-d_o}{Re(P_f-t_f)}\right)^{0.2}\right] \quad (1)$$

The pressure drop values for each cell are then converted to an equivalent force by multiplying with the bundle frontal area, and further to a momentum source term by dividing by the bundle volume.

Thirdly, the heat transferred to the air flowing through the tube bundle is modelled using an energy source term. The heat transferred between the sCO_2 and air for each sCO_2-side element is calculated by the Python script, which then writes these values to a text file in a specific order. The Python script uses *PyFluent* to instruct ANSYS Fluent to run another UDF. This UDF reads the heat transfer values from the text file and converts them to an energy source term by dividing by the volume of the sCO_2-side element. The UDF then assigns these energy source term values to the corresponding air-side mesh cells.

To simplify the air-side flow field solution further, the fan is modelled using the Frozen Rotor approach. This approach effectively fixes the tangential position of the two fan rotors during the simulation. A local reference frame is defined for each rotor sub-domain, which is specified to be rotating at the same speed and the same rotation origin as the fans, allowing flow to be approximated as steady.

With these simplifications in mind, the RANS equations are solved in the CFD model, with flow being considered compressible and steady in the relative frame of reference. The equation for energy conservation is also solved. Air is modelled as a real gas to account for fluid properties changes as the temperature increases through the bundle, using the NIST Real Gas option in ANSYS Fluent. Turbulence is modelled using the realizable k-epsilon model and enhanced wall treatment. The operating pressure is set to a value of 100000 Pa (1 bar).

All wall surfaces are set to no-slip wall boundary conditions. The interfacing surfaces between all mesh sub-domains, and between the two fan units, are connected using standard mesh interfaces. The remaining surfaces in the two inlet sub-domains are specified as pressure inlet boundary conditions, with the gauge total pressure set to 0 Pa and temperature to 15°C. For the two outlet sub-domains, the

remaining surfaces are set to pressure outlet boundary conditions, with the backflow gauge pressure set to 0 Pa and temperature to 15°C.

The SIMPLE pressure-velocity coupling scheme is used. For spatial discretisation, Least Squares Cell Based is used for gradient, PRESTO! for pressure, and QUICK for momentum, turbulent kinetic energy, turbulent dissipation rate and energy. The under-relaxation factors are set to 0.175 for momentum and 0.25 for energy. All other under-relaxation values are set to the default values suggested by ANSYS Fluent.

To validate the air-side setup, a simplified computational domain is used. Table 1 compares the temperature rise of the air in this simplified computational domain to that specified by Deshmukh et al. [2], with the air being modelled both with constant fluid properties and as a real gas. The close correlation between the results demonstrates that the modelling of the heat transferred to the air works as intended.

Table 1 also compares the static pressure drop of the air in this simplified domain to that predicted by the empirical correlation of Ganguli [10]. The good agreement between the constant fluid properties variant and Ganguli's correlation demonstrates that the modelling of the pressure drop also works as intended. However, the real gas variant predicts a significantly higher static pressure drop compared to the model using constant properties. This is due to the density of the air being reduced as it is heated, which accelerates the flow and leads to higher frictional losses.

Table 1: Comparison of air-side static pressure drop and temperature rise through the tube bundle

Model	Δp (Pa)	ΔT (°C)
Ganguli [10], Deshmukh et al. [2]	115.1	81.20
Simplified model with constant fluid properties	115.1	81.27
Simplified model with real gas properties	136.6	81.19

sCO_2-SIDE MODEL

The sCO_2 flow inside the tube bundle is modelled using the Thermofluid Network Method (TNM) of Laubscher et al. [6], implemented in a Python script. Flow is assumed to be incompressible, since Mach numbers well below 0.3 are expected. The TNM firstly discretises the sCO_2 flow path into one-dimensional elements, which are control volumes with only one inlet and outlet, and zero-dimensional nodes, which represent connections between the elements and can have multiple inlets and outlets.

Figure 2 illustrates how the flow is discretised in the y- and z-directions, along the length of an individual tube. To discretise the bundle in the x-direction, the bundle is divided into "blocks of tubes", each of which contains an equal number of tubes. It is then assumed that the sCO_2 flow inside of all tubes contained within a particular block are identical. Figure 2 gives an example of the resulting thermofluid network, with the bundle divided into five tube blocks.

The TNM applies the principles of conservation of mass and energy at each node, and conservation of linear momentum to each element, which defines three sets of equations. The TNM then solves the mass flow rates in each element, the stagnation pressures at each node, and the stagnation enthalpies at each node which simultaneously satisfies all three sets of equations. To achieve this, the solution procedure makes an initial guess of the sCO_2 flow field parameters, after which it continuously loops through a set of functions. Each function updates a portion of the flow field parameters. The Python script evaluates whether the required residuals have been achieved after each loop, allowing the sCO_2-side solution procedure to stop only upon meeting these criteria.

The first sCO_2 solution function updates the sCO_2 fluid properties at each node, as follows: the

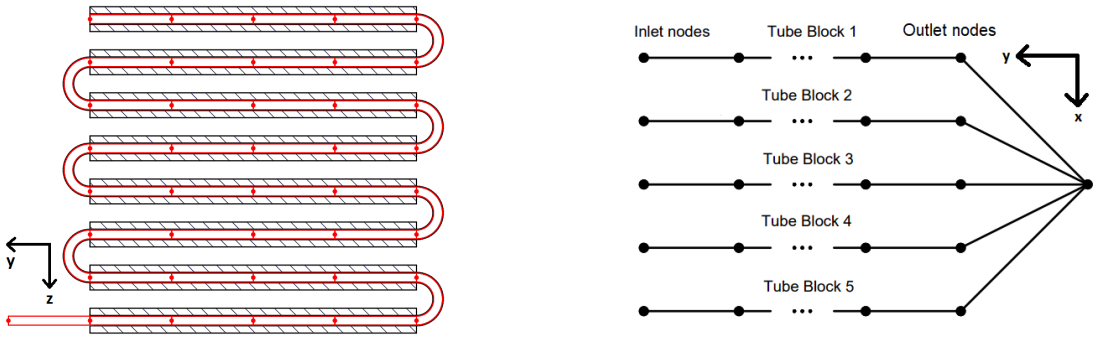

Figure 2: Thermofluid network model layout of sCO_2 flow in the tube bundle (not to scale)

entropy (s), velocity (u), static enthalpy (h), static pressure (p) and density (ρ) of the sCO_2 at a particular node is determined using:

$$s = f(h_0, p_0) \qquad u = \frac{\dot{m}_{per\,tube}}{\rho A_i} \qquad h = h_0 - \frac{u^2}{2} \qquad p = f(s,h) \qquad \rho = f(h,p) \tag{2}$$

where f indicates that the *CoolProp* module is used with the inputs given in brackets. The Python script uses the *fsolve* function to solve these equations simultaneously. The dynamic viscosity (μ), thermal conductivity (k) and specific heat capacity (c_p) of the sCO_2 at a particular node can then be calculated with the *CoolProp* module, using:

$$\mu = f(h,p) \qquad k = f(h,p) \qquad c_p = f(h,p) \tag{3}$$

The second sCO_2 solution function updates the sCO_2 friction factors in each element. For this purpose, the Reynolds number in each element is calculated using:

$$Re = \frac{\rho d_i u}{\mu} \tag{4}$$

The Darcy friction factor is then calculated using the Blasius correlation [5], expressed as:

$$f_D = 0.316 Re^{-\frac{1}{4}} \; for\; Re < 20000 \quad or \quad f_D = 0.184 Re^{-\frac{1}{5}} \; for\; Re > 20000 \tag{5}$$

The third sCO_2 solution function updates the sCO_2 mass flow rate in each element and the stagnation pressure at each node. Since the set of nodal mass balance equations alone does not have a singular, unique solution, the nodal mass and elemental momentum balance equations must be solved simultaneously (coupled solution). For each node along a tube length, the mass balance equation is defined as:

$$\dot{m}_{out} - \dot{m}_{in} = 0 \tag{6}$$

For the final outlet node in the bundle, which receives the flow leaving all tube blocks, the mass balance equation is expressed as:

$$\sum \dot{m}_{tube\,block\,outlets} - \dot{m}_{BC} = 0 \tag{7}$$

where $\dot{m}_{BC}$ is a boundary condition representing the mixed, uniform flow leaving the tube bundle. This boundary condition is always set to a value of 203.9 kg/s, which is the design point sCO_2 mass flow rate specified by Deshmukh et al. [2] for this ACHE, divided by three to account for the computational domain being only a third of the bundle. For each element along a tube length, the momentum balance equation is given by:

$$p_{0,out} - p_{0,in} + f_D u^2 \frac{\rho}{2} \frac{l}{d} = 0 \tag{8}$$

Finally, at each inlet node, a stagnation pressure boundary condition is defined, using:

$$p_{0,tube\ block\ inlet} - p_{BC} = 0 \tag{9}$$

where p_{BC} is always set to a value of 7.653 MPa, which is the design point sCO_2 pressure at the tube bundle inlet specified by Deshmukh et al. [2]. With the mass and momentum balance equations defined, the *fsolve* function is used to solve the equations simultaneously.

The fourth sCO_2 solution function updates the stagnation enthalpy at each node by solving the energy balance equations. For each node along a tube length, the energy balance equation is represented by:

$$(\dot{m}h_0)_{out} - (\dot{m}h_0)_{in} - \dot{Q} = 0 \tag{10}$$

where the calculation of the heat transfer rate ($\dot{Q}$) is discussed later in the paper. For the final outlet node in the bundle, which receives the flow leaving all tube blocks, the energy balance equation is formulated as:

$$\sum (\dot{m}h_0)_{tube\ block\ outlets} - \dot{m}_{BC}\, h_{0,mixed\ outlet} = 0 \tag{11}$$

At each inlet node, a stagnation enthalpy boundary condition is applied, using:

$$h_{0,tube\ inlet} - h_{BC} = 0 \tag{12}$$

where h_{BC} is set to the enthalpy corresponding to the design point temperature and pressure at the tube bundle inlet from Deshmuhk et al. [2], given as 111.2°C and 7.653 MPa. Since the enthalpy values are known at the inlet of each tube block, and the mass flow rate and heat transfer rate in each element have been calculated above, this set of energy balance equations can be solved simply by calculating the enthalpies from the inlet to the outlet nodes. The corresponding temperature values can then be found using the *CoolProp* module.

To validate the sCO_2-side model, the results are compared with that of a similar model in the Flownex Simulation Environment. The tube bundle is split into three tube blocks, with a different arbitrary heat transfer rate assigned to each. The results are compared in Table 2. The strong correlation seen between the two models demonstrate that the sCO_2 flow model works as intended.

Table 2: Comparison of sCO_2 results for Python TNM and Flownex model

Model/Block	$\dot{Q}$ (MW)	$\dot{m}$ (kg/s)	p_{out} (MPa)	T_{out} (°C)
Current/Block 1	0	60.98	7.473	110.2
Current/Block 2	5.822	67.89	7.473	52.40
Current/Block 3	11.64	75.00	7.473	32.81
Flownex/Block 1	0	60.97	7.474	110.2
Flownex/Block 2	5.822	67.86	7.474	52.38
Flownex/Block 3	11.64	75.04	7.474	32.83

HEAT TRANSFER MODEL

As noted before, the tube bundle is split into a number of elements. For the sCO_2-side, these elements are control volumes which represent the flow inside the tubes of a particular tube block. For the air-side, these elements are control volumes which represent the flow around the outside of the tubes in the tube block. The heat transferred between the two fluids in each element is solved using an iterative procedure, implemented in the Python script.

Accessing the required sCO_2 flow field parameters is simple, since the Python script stores these values in lists which are updated as the solution continues. To access the required air-side flow parameters, however, the values must be obtained from the ANSYS Fluent CFD simulation. The *PyFluent* module is therefore used to define a set of points in the CFD simulation, with each point representing the centre of a tube bundle element. When required, *PyFluent* is used to read the air-side conditions at each of these points, which are then stored in Python lists.

The heat transfer rate in each element is then calculated using the method by Kröger [11], as follows: The Prandtl number, Nusselt number and heat transfer coefficient of the sCO_2 in each element is calculated using the Gnielinski correlation [2, 5, 12], and Reynolds numbers from Equation 4:

$$Pr = \frac{c_p \mu}{k} \qquad Nu = \frac{(f_D/8)\,(Re - 1000)\,Pr}{1 + 12.7\,(f_D/8)^{0.5}\left(Pr^{2/3} - 1\right)} \qquad h_{sCO_2} = \frac{Nu\,k}{d_i} \tag{13}$$

After the air-side conditions have been obtained using *PyFluent*, the Reynolds number for the air in each tube bundle element is calculated using:

$$Re = \frac{\rho\, v_{crit}\, d_o}{\mu} \qquad v_{crit} = v_{free}\frac{A_{free}}{A_{crit}} \tag{14}$$

where v_{free} is the air velocity obtained from ANSYS Fluent, A_{free} is the tube bundle frontal area, and A_{crit} is the critical (minimum) flow area through the bundle. The air-side Prandtl number, Nusselt number and heat transfer coefficient in each element are then calculated using the correlation by Briggs and Young [13]:

$$Pr = \frac{c_p \mu}{k} \quad Nu = 0.134 Pr^{0.33} Re^{0.681}\left[\frac{2(P_f - t_f)}{d_f - d_r}\right]^{0.2}\left[\frac{P_f - t_f}{t_f}\right]^{0.1134} \qquad h_{air} = \frac{Nu\,k}{d_o} \tag{15}$$

Next, the geometric parameters must be calculated. The air- and sCO_2-side surface areas for each element are calculated using:

$$A_{air} = \left[\pi d_o\left(P_f - t_f\right) + 2 \times \frac{\pi}{4}\left(d_f^2 - d_o^2\right) + \pi d_f t_f\right]\frac{L_{Element}}{P_f} \qquad A_{sCO_2} = \pi d_i L_{element} \tag{16}$$

The fin efficiency is calculated using the correlation by Schmidt and Zeller [5]:

$$\eta_f = \frac{\tanh\left(\frac{b d_o \phi}{2}\right)}{\frac{b d_o \phi}{2}} \qquad b = \left(\frac{2h_{air}}{k_{aluminium} t_f}\right)^{0.5} \qquad \phi = \left(\frac{d_f}{d_o} - 1\right)\left[1 + 0.35\ln\left(\frac{d_f}{d_o}\right)\right] \tag{17}$$

The finned surface effectiveness can then be calculated using the correlation by Kröger [11]:

$$\varepsilon_{surface} = 1 - \left(1 - \eta_f\right)\left(\frac{A_{fin}}{A_{fin} + A_{root}}\right) \tag{18}$$

The overall heat transfer coefficient and heat transfer rate for each element can be found using:

$$UA = \left(\frac{1}{h_{sCO_2} A_{sCO_2}} + \frac{\ln\left(\frac{d_o}{d_i}\right)}{2\pi k_{steel} L_{element}} + \frac{1}{h_{air} A_{air} \varepsilon_{surface}}\right)^{-1} \tag{19}$$

$$\dot{Q} = UA(T_{sCO_2} - T_{air}) \times N_{Tubes/Block} \tag{20}$$

Finally, once the heat transfer rates for all elements have been calculated, they are written to the text file, as mentioned in the air-side model section above.

CO-SIMULATION PROCEDURE

The Python co-simulation script starts by reading the initialised air-side case and data files from ANSYS Fluent. The heat transfer rates in all elements are initially set to zero, and the sCO_2-side flow field is solved. With both sides of the co-simulation initialized, the overall co-simulation procedure starts, which loops through the following steps until the solution has converged: *PyFluent* accesses the air-side conditions in each element from ANSYS Fluent; the heat transfer rates in each element are calculated and written to a text file; the sCO_2-side flow field is solved; *PyFluent* instructs ANSYS Fluent to use the UDF, which reads the heat transfer rate text file, converts them to energy source terms, and assigns them to the air-side mesh cells; *PyFluent* instructs ANSYS Fluent to run a number of air-side solution iterations.

RESULTS

For the full thermal ACHE co-simulation, the computational domain is split into twelve tube blocks, and each tube pass is split into sixteen sections. The air-side mesh uses 19.16×10^6 cells. These results were compared with two coarser co-simulations, which produces similar results. Therefore, the results are not sensitive to the selected discretisation resolution.

Overall performance

Table 3 provides the main ACHE thermal performance results, and compares these values to the design point values specified by Deshmukh et al. [2]. The overall heat transfer rate is seen to be significantly below the design point value. Consequently, the average sCO_2 outlet temperature is higher than the required value.

Table 4 compares the fan performance values for both fans within the co-simulation to that of the isothermal model of Boshoff et al. [9]. The cooling air flow rates obtained are below that of the isothermal model, which is likely due to the current model accounting for the heat transferred to the air. As demonstrated in Table 1, this results in an increase in static pressure drop through the bundle. As a result, the fans operate further from their design point flow rate of 175.7 m^3/s, which reduces their efficiency. The reduced cooling air flow rate also contributes to the low heat transfer rate seen in Table 3.

Table 3: ACHE overall thermal performance results

Method	$\dot{Q}_{ACHE}$ (MW)	$T_{sCO_2,out}$ (°C)
Design point	104.8	32.10
Co-simulation	83.34	35.61

Table 4: Fan aerodynamic performance results

Method	$\dot{V}_F$ (m^3/s)	Δp_{ts} (Pa)	P_F (kW)	η_{ts} (%)
Design point	175.7	-	-	-
Isothermal model [9]	169.4	110.5	31.91	58.66
Co-simulation, Fan 1	157.3	117.0	33.13	55.55
Co-simulation, Fan 2	157.2	117.1	33.10	55.61

sCO_2 conditions in each tube block

An investigation of the results for the individual tube blocks demonstrates that the sCO_2 mass flow rates and outlet temperatures are distributed in a symmetrical pattern. This is due to the non-uniform cooling air velocity profile provided by the two fans, which results in higher heat transfer rates over tubes directly downstream of the fan blades, and lower heat transfer rates behind the fan hubs and towards the sides of the bundle. The sCO_2 mass flow rates are therefore seen to range from 16.83 kg/s for the tube blocks downstream of the hub, to 17.15 kg/s for tube blocks downstream of the blades.

Flow conditions along the tube length

Figure 3 illustrates the distributions of heat transfer rate and sCO_2 temperature in each tube block. The results for each tube block are coloured based on their distance from the x-axis origin (at the centre of the fans). The heat transfer rates are seen to vary between blocks, with the tube blocks closer to the centre achieving higher heat transfer rates. This is caused by the higher air velocities downstream of the fan. Note that, since the sCO_2 pressures at the inlet and outlet of each tube block are identical, the sCO_2 pressure distributions in each tube block are also nearly identical, regardless of the non-uniform cooling.

The resulting temperature distributions, however, are seen to differ between blocks, with tube blocks close to the centre having lower outlet temperatures. As a result, the sCO_2 leaving the central tube blocks are closer to the critical point. Due to the overall heat transfer rate achieved being below the design value, the sCO_2 in all tube blocks remains well above the critical temperature, meaning there is no risk of the sCO_2 ceing cooled below the critical point.

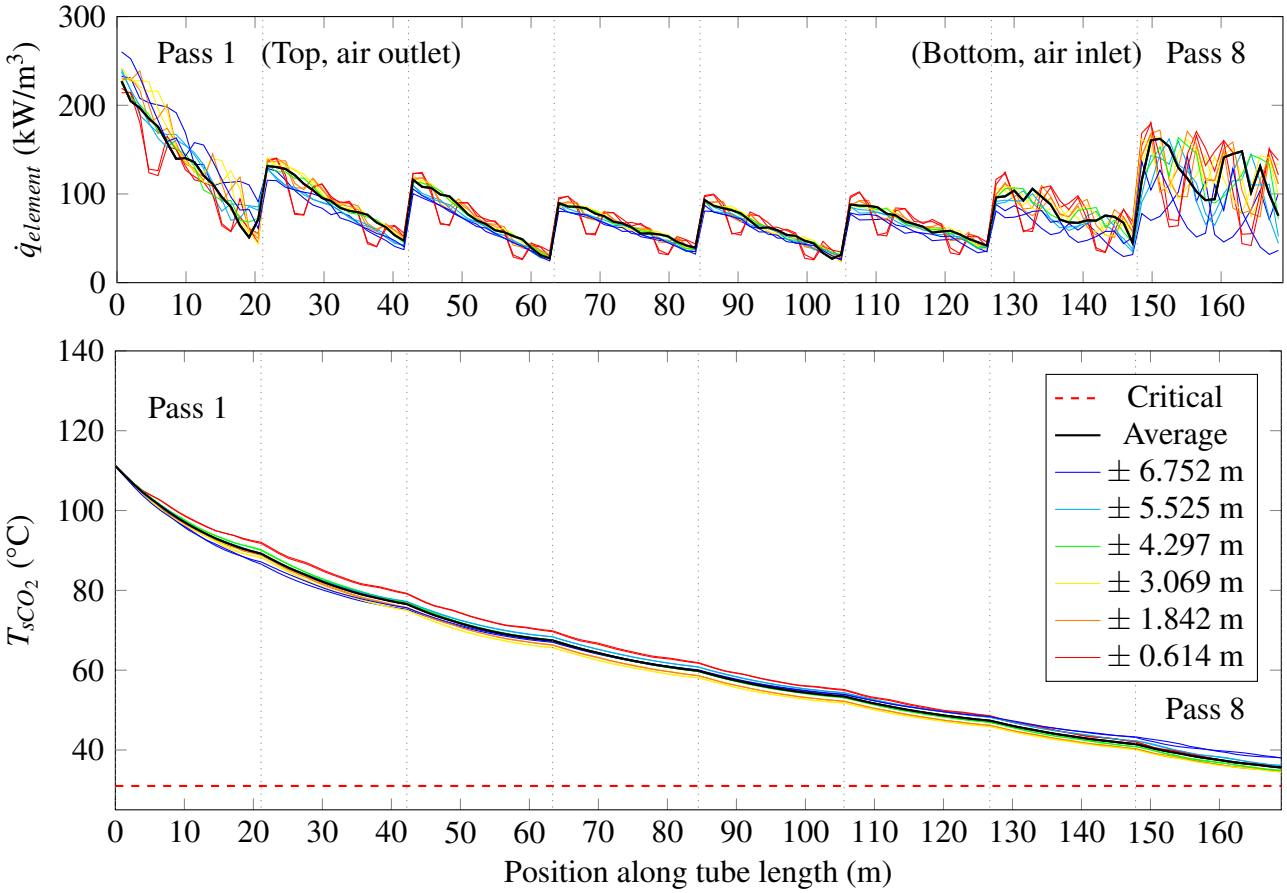

Figure 3: Heat transfer rate and sCO_2 temperatures in each tube block

CONCLUSIONS AND RECOMMENDATIONS

The co-simulation demonstrates that the heating of the air significantly increases the air's static pressure drop through the finned-tube bundle. Since this effect was not accounted for by the fan design procedure, the operating point flow rate achieved by each fan is 18.5 m^3/s (10.5%) below the required value. Further, the co-simulation predicts that the overall heat transfer rate achieved by the ACHE is 21.5 MW (20.5%) below the required value, partly due to the low cooling air flow rate. As a result of the low heat transfer rate, the sCO_2 leaving the tube bundle and entering the compressor is further from the critical point than intended, and therefore less dense. This will most likely result in the power cycle's efficiency being reduced.

The results indicate that the sCO_2 in tubes downstream of the high velocity air leaving the fan blades are at a lower temperature. Due to the low overall heat transfer rate achieved however, the sCO_2 temperature is still well above the critical point. If the overall heat transfer rate achieved was closer to the design value, and was applied non-uniformly, the sCO_2 in some tubes could very well be cooled below the critical point. To avoid this, the uniformity of the cooling air distribution provided by the fans could be improved. However, since the sCO_2 leaving all tubes are mixed, the sCO_2 should return to the supercritical state before leaving the ACHE. The effect of non-uniform cooling on the entire power cycle is therefore not as significant. Instead, it is important to ensure that the overall heat transfer rate does not exceed the design point value significantly, as this could result in the overall outlet conditions being sub-critical, which would most likely cause a large reduction in the power cycle's efficiency.

ACKNOWLEDGEMENTS

The authors would like to acknowledge the following groups and individuals for their contribution towards the completion of this work: The Solar Thermal Energy Research Group at Stellenbosch University for their ongoing support. Prof Alessandro Corsini, Prof Giovanni Delibra and Dr Lorenzo Tieghi from Sapienza University of Rome, for their guidance during the early stages of the work, and the Centre for High Performance Computing, South Africa, for providing computational resources to this research project. This work is based on the research supported in part by the National Research Foundation of South Africa (grant no KIC240821261750).

REFERENCES

[1] V. Dostal, P. Hejzlar, and M. J. Driscoll, "High-performance supercritical carbon dioxide cycle for next-generation nuclear reactors," *Nuclear Technology*, vol. 154, no. 3, 2006.

[2] A. Deshmukh, J. Kapat, and A. Khadse, "Transient thermodynamic modeling of air cooler in supercritical CO2 Brayton cycle for solar molten salt application," in *Proceedings of the ASME Turbo Expo 2019: Turbomachinery Technical Conference and Exposition*, (Phoenix, Arizona), 2019.

[3] K. Brun, P. Friedman, and R. Dennis, *Fundamentals and applications of supercritical carbon dioxide (sCO2) based power cycles*. Cambridge: Elsevier Science & Technology, 2017.

[4] A. Moisseytsev, Q. Lv, and J. J. Sienicki, "Dry Air Cooler Modeling for Supercritical Carbon Dioxide Brayton Cycle Analysis," tech. rep., Argonne National Laboratory - Nuclear Engineering Division, 2016.

[5] A. Lock, K. Hooman, and Z. Guan, "A detailed model of direct dry-cooling for the supercritical carbon dioxide Brayton power cycle," *Applied Thermal Engineering*, vol. 163, 2019.

[6] R. Laubscher, P. Rousseau, J. Van der Spuy, C. Du Sart, and J. Pretorius, "Development of a 1D network-based momentum equation incorporating pseudo advection terms for real gas sCO2 centrifugal compressors which addresses the influence of the polytropic path shape," *Thermal Science and Engineering Progress*, vol. 55, no. October, pp. 1–13, 2024.

[7] F. D. Boshoff, S. J. Van der Spuy, J. P. Pretorius, and C. J. Meyer, "Design of an axial flow fan for a unique cooling application," in *Proceedings of the ASME Turbo Expo 2022: Turbomachinery Technical Conference and Exposition*, (Rotterdam, Netherlands), 2022.

[8] F. D. Boshoff, S. J. Van der Spuy, J. P. Pretorius, and C. J. Meyer, "Investigation into the predicted performance of a cooling fan for an sCO2 concentrated solar power plant," *Proceedings of the Institution of Mechanical Engineers, Part A: Journal of Power and Energy*, vol. 238, no. 5, 2024.

[9] F. D. Boshoff, S. J. Van der Spuy, and J. P. Pretorius, "Axial Flow Fan Performance in a Forced Draught Air-Cooled Heat Exchanger for a Supercritical Carbon Dioxide Brayton Cycle," *Journal of Engineering for Gas Turbines and Power*, vol. 147, no. 1, 2025.

[10] A. T. Ganguli, "Parametric study of air-cooled heat exchanger finned tubed geometry," *American Institute of Chemical Engineers Symposium Series*, vol. 81, no. 245, pp. 122–128, 1985.

[11] D. G. Kröger, *Air-cooled heat exchangers and cooling towers*. Tulsa, Okla: Penwell Corp., 2004.

[12] L. Abrahams, C. Du Sart, and R. Laubscher, "Design of an air-cooled heat rejection system for a sCO2 concentrated solar power plant," in *16th International Conference on Heat Transfer, Fluid Mechanics and Thermodynamics*, (Virtual), 2022.

[13] D. E. Briggs and E. H. Young, "Convection heat transfer and pressure drop of air flowing across triangular pitch banks of finned tubes," *Chemical Engineering Progress Symposium Series*, vol. 59, no. 41, pp. 1–10, 1963.

NOMENCLATURE

Abbreviations

ACHE	Air-cooled heat exchanger
CFD	Computational fluid dynamics
CSP	Concentrated solar power
RANS	Reynolds-averaged Navier-Stokes
sCO_2	Supercritical carbon dioxide
TNM	Thermofluid network model
UDF	User defined function

Variables

A	Area (m^2)
b	Placeholder
d	Diameter (m)

f	Friction factor, function
G	Mass velocity (kg/s·m^2)
H	Height (m)
h	Heat transfer coefficient (W/m^2·K), specific enthalpy (J/kg)
k	Thermal conductivity (W/m·K)
L	Length (m)
$\dot{m}$	Mass flow rate (kg/s)
N	Number of
P	Pitch (m), power (W)
p	Pressure (Pa)
$\dot{Q}$	Heat transfer rate (W)
$\dot{q}$	Heat transfer rate per unit volume (W/m^3), per unit length (W/m)
S	Source term
s	Specific entropy (J/kg·K)
T	Temperature (°C or K)
t	Thickness (m)
UA	Overall heat conductance (W/K)
V	Volume (m^3)
$\dot{V}$	Volumetric flow rate (m^3/s)
v	Velocity (m/s)
W	Width (m)
Δ	Change in
ε	Effectiveness
η	Efficiency (%)
μ	Dynamic viscosity (kg/s·m)
ρ	Density (kg/m^3)
ϕ	Placeholder

Subscripts

0	Stagnation
ACHE	Entire air-cooled heat exchanger
air	Air-side
aluminium	For aluminium
BC	Boundary condition
crit	Critical
D	Darcy
element	Element

F	Fan
f	Fin
fin	Fin
$free$	Free
fr	Frontal
i	Inner
in	Inlet
l	Longitudinal
o	Outer
out	Outlet
p	Constant pressure
t	Transverse
r	Rows
$root$	Root
$steel$	For steel
$surface$	Surface
ts	Total-to-static
z	z-component

Dimensionless numbers

Eu	Euler number
Nu	Nusselt number
Pr	Prandtl number
Re	Reynolds number